International Journal of Innovative
Computing, Information and Control
Volume **18**, Number **2**, April **2022**

ICIC International ©2022 ISSN 1349-4198
pp. 577–590

DEPTH MAP RESTORATION ALGORITHM BASED ON IMPROVED SUPER-RESOLUTION AND FMM BY USING WEIGHT FUNCTION

Xinyue Xu[1] and Qingjiu Huang[2,*]

[1]School of Information and Electronic Engineering
Zhejiang Gongshang University
No. 18, Xuezheng Street, Xiasha University Town, Hangzhou 310018, P. R. China
1255728907@qq.com

[2]Control System Laboratory
Graduate School of Engineering
Kogakuin University
1-24-2 Nishi-Shinjuku, Tokyo 163-8677, Japan
*Corresponding author: huang@cc.kogakuin.ac.jp

Received August 2021; revised December 2021

Abstract. *With the advancement of intelligence in manufacturing, the depth information obtained by depth cameras is widely used in various fields of manufacturing. However, the depth map obtained by low-resolution depth cameras that are affordable to small and medium-sized manufacturing has problems that are low resolution and missing depth information. Therefore, this study proposes a depth map restoration algorithm based on improved super-resolution and FMM (Fast Marching Method) by using weight function, which is to improve the resolution of low-resolution depth cameras and repair the missing depth information. First, a high-resolution depth map is obtained by super-resolution processing of the low-resolution depth map. Then, the depth information of the enhanced high-resolution depth map is restored by the improvement of the weight function of FMM. In addition, super-resolution processing is used again to repair the missing depth information of the edge caused by the improved FMM. Finally, the effectiveness of this study for depth information restoration during image enhancement is shown by an experiment which down-samples a depth map of 300,000 pixels taken by a binocular depth camera, then doubles the resolution and repairs the depth information at the same time.*

Keywords: Depth map restoration, Super-resolution of the depth map, FMM (Fast Marching Method), Improved weight function, Experiment

1. **Introduction.** With the development of science and technology, depth information is widely used in areas such as 3D reconstruction and augmented reality [1]. At present, depth information is mainly obtained by depth cameras with structured light or TOF (Time of Flight) technology. However, the depth map obtained by low-resolution depth cameras that are affordable by small and medium-sized manufacturing has problems that are low-resolution and missing depth information. Therefore, how to effectively enhance the depth map obtained by low-resolution depth cameras to high resolution and repair the missing depth information has broad market needs.

Regarding the study of depth map restoration, there is a restoration processing algorithm that performs hierarchical sequencing of depth missing regions by adding joint bilateral filtering [2,3], which has good results for local regions, but is not ideal for restoration in edge regions and cannot repair globally the missing depth information of images. Therefore, there is also a restoration algorithm for the missing depth information through the

DOI: 10.24507/ijicic.18.02.577

design of interpolation weight functions [4,5], which makes the good effect of restoration of the missing depth information in edge and overall, and achieves global depth information restoration of images. However, the value of the balance factor of weights is not well controlled, which makes this algorithm difficult to make practical. There are also restoration algorithms that deal with depth information discontinuity area by modeling the smoothing term [6,7], which works well for depth restoration in-depth information discontinuity regions, but the modeling process is very complex which also makes this algorithm difficult to make practical. There is also an image restoration algorithm that restores images by enhancing image features in the pre-processing stage and then applying deep learning to the image [8], which is more effective for images with obvious image features that are missing information, but less effective for images with less obvious features. Therefore, there is also an algorithm for restoration of depth maps by designing depth selectivity and saliency fusion networks [9], which not only avoid learning ambiguities caused by the conflict of feature but also improve the depth quality. However, the fusion balance between selectivity and saliency needs to be improved. There is also an algorithm that uses semantic guidance modules and multi-scale adaptive fusion for depth maps restoration [10], which allows for reduced hardware consumption while ensuring image restoration accuracy, but still requires high hardware conditions. Therefore, there is also a fast depth-completion algorithm that makes use of multiple custom kernels for inflation [11], which use only traditional image processing techniques and require fewer hardware conditions, while outperforming several deep learning algorithms in terms of effectiveness but are unable to repair large areas of depth deficit. There is also an algorithm for categorizing voids by fuzzy inference [12], which allows images with complex geometric features to be restored efficiently, but only for certain types of models and is not very robust. In summary, dealing with global depth information restoration of images is the key technology on how to effectively enhance depth maps acquired by low-resolution depth cameras to high resolution, and repair missing depth information.

Therefore, this study proposes a depth map restoration algorithm based on improved super-resolution and FMM (Fast Marching Method) by using weight function, which is to improve the resolution of low-resolution depth cameras and repair the missing depth information.

Firstly, the depth map is processed for super-resolution. Specifically, a high-resolution depth map is obtained by bicubic interpolation of a low-resolution depth map. Moreover, to retain the high-frequency information at the edges of the image, an adaptive weight function of the window is constructed for the guided filtering function to update the depth information after an interpolation. Then, a cost function of depth information prediction is constructed by the L2 norm. In addition, the final value of the super-resolution pixel can be obtained by fitting a quadratic polynomial between the minimum of the cost function and the depth information updated by the guided filtering.

Secondly, FMM is used to repair the missing depth information. Specifically, a new weight function of FMM is created by using the distance coefficients and color coefficients of the bilateral filtering of RGB images to suppress the over smoothing of depth information of corners. In addition, the created weight function is substituted into the estimation equation of depth information of FMM to repair the missing depth information.

Then, the above super-resolution process is used again to repair the missing depth information of edges caused by the FMM processing; thus, the global repairing of depth information is achieved.

Finally, the effectiveness of this study for depth information restoration during image enhancement is shown by an experiment which down-samples a depth map of 300,000

pixels taken by a binocular depth camera, then doubles the resolution and repairs the depth information at the same time.

2. **Related Work.** The restoration of images is divided into restoration at the texture of the image and restoration at the structure of the image. On the one hand, as the depth map is mainly obtained by the position of the camera to the object, most of the actual depth maps are taken concerning the structure of the object. On the other hand, when influenced by the color, material, or even the environment of the object, the depth information may be missing from the depth map. Furthermore, the location of the missing depth information is most likely to occur in the structure of the image. However, most of the algorithms mentioned in the first section are unable to effectively restore the missing depth information at low resolution and over large areas. Therefore, to better preserve the image resolution while depth restoration, this study improves the guided filtering in Section 2.1 and uses the method in Section 3.1 for super-resolution reconstruction. Moreover, the missing information at the structure of the depth map is repaired in combination with the FMM algorithm improved by Section 2.2 in Section 3.2.

2.1. **Guided filtering.** The guided filtering can be described as an edge-holding filter that obtains the output graph q_i by using the input graph p_i and the guided graph I_i to reduce the noise of the input graph p_i [13]. Here, the guided graph I_i is similar to the input graph p_i in structure.

First, as shown in Equation (1), establish the relationship between the input graph p_i and the output graph q_i. Here, n_i is noise. Secondly, as shown in Equation (2), establish the relationship between the guide map I_i and the output map q_i. Here, i is the position of the pixel in the window w_k, k is the central pixel of the window w_k and a_k, b_k are linear coefficients.

If the input graph p_i contains less noise, the better the quality of the output graph q_i. Therefore, Equations (1) and (2) are combined and transformed into a regularization problem as shown in Equation (3), where ε is the regularization parameter used to prevent a_k from being too large and pixels from being over-smoothed.

Then, the parameters a_k and b_k are obtained by solving Equation (3) by the least-squares method as shown in Equations (4) and (5). Here, $\mathrm{cov}_k(I,p)$ is the covariance between the guidance image I_i and input image p_i within the window w_k as shown in Equation (6). $\delta_{I,k}^2$ is the variance of the guidance image I_i within w_k as shown in Equation (7). In addition, in Equation (6), M is the number of pixels within a window w_k and $\overline{I_k}$, $\overline{p_k}$ are the mean values of the guidance image I_i and input image p_i within the window w_k which respectively are shown in Equations (8) and (9).

$$q_i = p_i - n_i \tag{1}$$

$$q_i = a_k I_i + b_k, \quad \forall i \in w_k \tag{2}$$

$$E(a_k, b_k) = \sum_{i \in w_k} \left((a_k I_i + b_k - p_i)^2 + \varepsilon a_k^2 \right) \tag{3}$$

$$a_k = \frac{\mathrm{cov}_k(I,p)}{\delta_{I,k}^2 + \varepsilon} \tag{4}$$

$$b_k = \overline{p_k} - a_k \overline{I_k} \tag{5}$$

$$\mathrm{cov}_k(I,p) = \frac{1}{M} \sum_{i \in w_k} \left\{ \left[I_i - \overline{I_k} \right] \left[p_i - \overline{p_k} \right] \right\} \tag{6}$$

$$\delta_{I,k}^2 = \frac{1}{M}\sum_{i\in w_k}\left[I_i - \overline{I_k}\right] \tag{7}$$

$$\overline{I_k} = \frac{1}{M}\sum_{i\in w_k} I_i \tag{8}$$

$$\overline{p_k} = \frac{1}{M}\sum_{i\in w_k} p_i \tag{9}$$

2.2. **Basic principle of the FMM algorithm.** The FMM algorithm first specifies a window B_z of size $N \times N$, which is centered on the unknown pixel z on the boundary of the damaged region of the image, and establishes the relationship equation between the known pixel t and the unknown pixel z shown in Equation (10) to recover the value of the unknown pixel z. During the recovery process, a weighted average of all known pixel t within the window B_z is performed using the weight function W_{FMM} as shown in Equation (11).

Next, the value D_Z of the unknown pixel is obtained from Equation (12). Finally, it is gradually expanded towards the interior of the damaged region until the repair is completed [14]. The repair in order of pixels is determined by the distance from the pixel to the initial edge, and the closer the distance is, the more priority is repaired.

The weight function W_{FMM} is composed of three components. The first component is the weight W_{dir} of the direction of the boundary normal of pixel t near pixel z as shown in Equation (13), the second component is the weight W_{dis} of the distance from pixel t to pixel z as shown in Equation (14), and the third component is the weight W_{lev} reflecting the relationship between the distance from point t to the initial edge and the distance from pixel z to the initial edge as shown in Equation (15).

$$D_z = D_t + \nabla D_t(z - t) \tag{10}$$

$$W_{FMM} = W_{dir}W_{dis}W_{lev} \tag{11}$$

$$D_Z = \frac{\sum_{t\in B_z} W_{FMM}[D_t + \nabla D_t(z - t)]}{\sum_{t\in B_z} W_{FMM}} \tag{12}$$

$$W_{dir} = \frac{z - t}{\|z - t\|}N(z) \tag{13}$$

$$W_{dis} = \frac{1}{\|z - t\|^2} \tag{14}$$

$$W_{lev} = \frac{1}{1 + |T(z) - T(t)|} \tag{15}$$

3. **An Algorithm Combining Super-Resolution with FMM Based on the Improved Weight Function.** This study combines a super-resolution algorithm with FMM based on the improved weight function for depth map restoration. As shown in the algorithm flowchart of Figure 1, the inputs of this algorithm are the low-resolution depth map D and the high-resolution RGB image D1, and the output is the final repaired depth map D5. The algorithm in this study is mainly divided into three parts. Firstly, the low-resolution depth map D is super-resolved to obtain the image-enhanced high-resolution depth map D2.

Next, the depth information of the image-enhanced high-resolution depth map is restored by improving the weight function of the FMM. Finally, the super-resolution processing is used again to repair the missing depth information at the edge caused by the improved FMM.

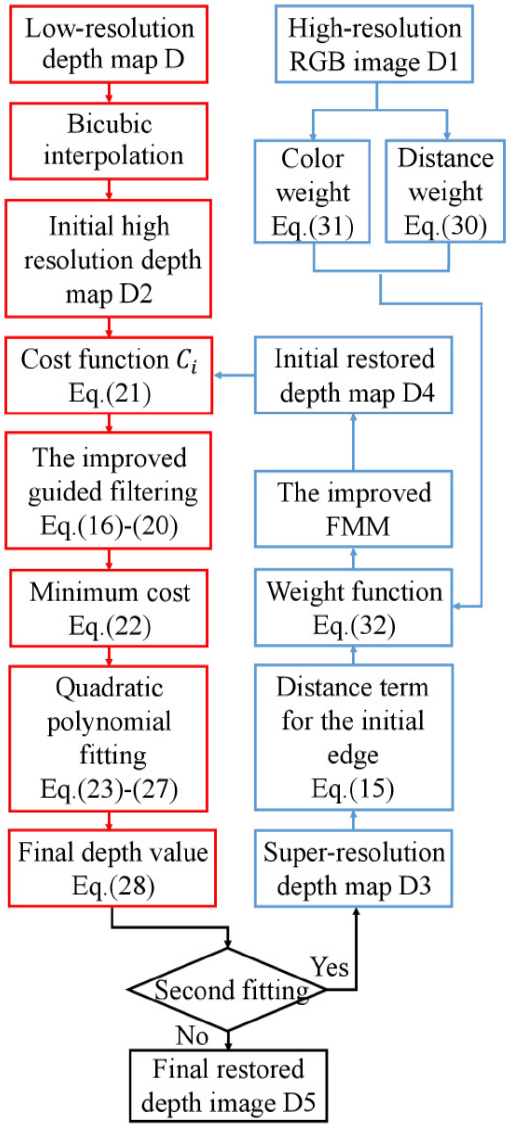

FIGURE 1. Flowchart of the algorithm for this study

Section 3.1 and Section 3.2 of this study respectively give detailed descriptions of the super-resolution reconstruction based on guided filtering and the improved FMM image restoration algorithm.

3.1. **Super-resolution reconstruction based on guided filtering.** In this study, we improve the guided filtering to achieve super-resolution reconstruction. The specific steps are shown as follows.

3.1.1. *Creating adaptive window weights.* According to the traditional guided filtering algorithm described in Section 2.1, the coefficients a_k and b_k are obtained by taking the mean value of all pixels in the window w_k, and such an assignment will cause misjudgment of pixels in edge regions. To solve this problem, the larger weights should be assigned in edge regions, and the smaller weights should be assigned in non-edge regions in a window. However, the difference $|SSIM_{I_i} - SSIM_{p_i}|$ of the Structural Similarity Index Measure (SSIM) between pixels is larger in the edge region and smaller in the smooth region. Using this feature, it is possible to realize the adaptive weight assignment of the window to make it more reasonable for pixel estimation in the edge regions. Therefore, as shown

in Equation (19), *SSIM* is used as the window weight in this study. Here, μ_I, μ_p, σ_I^2, σ_p^2 are the mean and variance of I_i, p_i respectively, and σ_{Ip} is the covariance of I_i and p_i.

3.1.2. *Designing adaptive smoothing factors.* The traditional guided filtering uses the same smoothing coefficient ε for all w_k. According to Equation (4), when $\delta_{I,k}^2$ is much smaller than ε, a_k will be close to 0. At this time, according to Equation (5), b_k will be close to $\overline{p_k}$. And according to Equation (2), $q_i = \overline{p_k}$. When $\delta_{I,k}^2$ is much larger than ε, a_k will be close to 1. At this time, b_k will be close to 0. And according to Equation (2), $q_i = I_i$. Therefore, the fixed smoothing coefficient ε will cause the estimated value q_i to be over-smooth or under-smooth.

In this study, through the improvement of Equation (16), the Mean Absolute Error (*MAE*) between the true value and the estimated value is selected as the smoothing factor. When the true value is close to the estimated value, the smoothing term is smaller. On the opposite side, the smoothing term is larger. Therefore, the adaptive control is realized by the smoothness of the pixels in the window. The final obtained depth value Q_i is shown in Equation (20).

$$E(a_k, b_k) = \sum_{i \in w_k} \left((a_k I_i + b_k - p_i)^2 + \varepsilon MAE a_k^2 \right) \tag{16}$$

$$MAE = |q_i - I_i| \tag{17}$$

$$a_k = \frac{\mathrm{cov}_k(I, p)}{\delta_{I,k}^2 + \varepsilon MAE} \tag{18}$$

$$W = SSIM_{I_i p_i} = |SSIM_{I_i} - SSIM_{p_i}| = \frac{(2\mu_{I_i}\mu_{p_i} + c1)(2\sigma_{I_i p_i} + c2)}{\left(\mu_{I_i}^2 + \mu_{p_i}^2 + c1\right)\left(\sigma_{I_i}^2 + \sigma_{p_i}^2 + c2\right)} \tag{19}$$

$$Q_i = W \frac{\mathrm{cov}_k(I, p)}{\delta_{I,k}^2 + \varepsilon MAE} I_i + W\left(\overline{p_k} - a_k \overline{I_k}\right) \tag{20}$$

3.1.3. *Fitting quadratic polynomials.* To reduce the interference of noise on the pixel, minimize the error between the true value and the estimated value of the pixel, and make the pixel get a more accurate estimation, this study sets an initial cost C_i as shown in Equation (21) to let the cost be aggregated on the pixel. Here, d is the candidate depth of the pixel and $D2_i(x, y)$ is the depth of the current initial high-resolution depth map. Using the improved guided filtering, the cost C_i is aggregated as shown in Equations (16)-(20). The latest cost after aggregating is C_{new} shown in Equation (22). Moreover, since the stability of the higher-order polynomial is poor, a quadratic polynomial as shown in Equation (23) is used as the fitting function for estimating the pixels. To minimize the error of fitting, the minimal value $x_{\min}$ of Equation (23) needs to be found. Here, $x_{\min}$ is obtained by Equation (24). Since the coefficients a and b are unknown, it is difficult to solve $x_{\min}$ directly. Therefore, $F(x)$ is obtained by substituting the candidate depths d, $d-1$, $d+1$ into Equation (25). Then, the estimated depth $X_{\min t}$ as shown in Equation (27) is obtained by substituting the solution of Equation (26) into Equation (24) [15]. Finally, to make the estimated value more accurate, two depth information on the left and right sides is fitted four times according to the above method. In addition, the mean value $X'_{\min}$ of the fitting results is taken as the final depth estimates shown in Equation (28).

$$C_i = \frac{\left(d - D2_i(x, y)^2\right)}{2} \tag{21}$$

$$C_{new} = \frac{\left(d - Q_i(x, y)\right)^2}{2} \tag{22}$$

$$F(x) = ax^2 + bx + c \tag{23}$$

$$x_{\min} = -\frac{b}{2a} \tag{24}$$

$$F(x) = C_{new}x \tag{25}$$

$$\begin{cases} F(d) = ad^2 + bd + c \\ F(d-1) = a(d-1)^2 + b(d-1) + c \\ F(d+1) = a(d+1)^2 + b(d+1) + c \end{cases} \tag{26}$$

$$X_{\min t} = d - \frac{F(d+1) - F(d-1)}{2(F(d+1) + F(d-1) - 2F(d))} \tag{27}$$

$$X'_{\min} = \frac{X_{\min 1} + X_{\min 2} + X_{\min 3} + X_{\min 4}}{4} \tag{28}$$

3.2. **Improved FMM image restoration algorithm.** It can be seen from Equation (12) that the restoration quality of the FMM algorithm is directly related to the weight W_{FMM}. The traditional FMM algorithm only calculates the weight W_{FMM} for the regions with missing pixels in the image to estimate the missing pixels. However, depth maps generally contain missing depth information, and if only the information of the depth map is used in the restoration process, the weight W_{FMM} will be incorrectly estimated in the edge region where the depth information is missing, and subsequently affect the final estimation of the depth information. Therefore, to reduce the estimation error of the depth information in the edge regions, this study proposes an algorithm to improve the weight W_{FMM} by using the distance information and color information of the RGB image.

Since the weight function related to the distance information and the color information of bilateral filtering as shown in Equation (29) can better assign weights to pixels in the edge regions of the image [16], this study imports the distance weights and the color weights from bilateral filtering in the design of the weights. Specifically, Equation (14) is changed to a distance weight in bilateral filtering as shown in Equation (30), and a color weight as shown in Equation (31) is added. Here, t' and z' respectively correspond to the values of pixel t and pixel z in the RGB image.

In addition, the color weight W_{color} gives more weight to pixels that are further away and have similar color than to pixels that are closer and have a large difference of color, while the normal weight W_{dir} gives more weight to pixels that are closer to the direction of the normal line. The two weights are relatively conflicting. Therefore, this study does not use normal weights W_{dir} in the calculation of the weights.

At the same time, according to the characteristics of the color weight W_{color} in the above analysis, it can be known that the weight W'_{FMM} cannot be designed into the form of $W_{dis}W_{color}W_{lev}$. Otherwise, in the edge regions with similar colors, when the color weight W_{color} is too large, the overall weight will be too large so that the pixels that should have been correctly estimated are incorrectly estimated. Therefore, the weight function W'_{FMM} is designed as Equation (32) in this study. Here, the parameter α is the fusion coefficient of the $W_{lev}W_{dis}^2$ term and the $W_{color}W_{dis}$ term. The parameter α serves to calculate the weights W'_{FMM} mainly with the weights W_{lev} and W_{dis} when the weights W_{color} within the window fluctuate widely. When the weight W_{lev} in the window fluctuates greatly, the weights W'_{FMM} are mainly with the weights W_{color} and W_{dis}.

The traditional FMM algorithm can quickly restore large areas of missing depth information. However, when a large area of depth loss occurs on the contours of an object, the depth map restored by the traditional FMM algorithm will show pseudo-edges and over-smoothed edge inflections in the area of missing information. The improved FMM

algorithm in this section suppresses the pseudo-contour phenomenon and enhances the edges when repairing large areas of missing depth information that occurs on the contours of the object. The improved FMM algorithm in this section suppresses the pseudo-contour phenomenon and enhances the edges when repairing large areas of missing depth information on object contours. Specific experimental results are presented in Section 4.2.

Next, Equation (32) is substituted into Equation (12) to obtain the initial restored depth map D4. Finally, as shown in the flowchart of Figure 1, the depth map D4 is again augmented with depth information by the algorithm of quadratic polynomial fitting with guided filtering described in Section 3.1 to obtain the final restored depth map D5.

$$W_b = \exp\left(-\frac{\|t-z\|^2}{2\sigma_{dis}^2} - \frac{\|t'-z'\|}{2\sigma_{color}^2}\right) \tag{29}$$

$$W_{dis} = \exp\left(-\frac{\|t-z\|^2}{2\sigma_{dis}^2}\right) \tag{30}$$

$$W_{color} = \exp\left(-\frac{\|t'-z'\|^2}{2\sigma_{color}^2}\right) \tag{31}$$

$$W'_{FMM} = (1-\alpha)W_{lev}W_{dis}^2 + \alpha W_{color}W_{dis} \tag{32}$$

4. **Results and Analysis of the Experiment.** To verify the effectiveness of this study on the depth information restoration algorithm in the image enhancement process, a depth image with a resolution of 640 × 480 was selected for the experiments. The operating system of the computer used in this experiment is Windows 8.1, the CPU is Intel (R) Core (TM) i5-5200u, the computer's main frequency is 2.20GHz, and the memory is 4GB. This experiment is programmed on the PyCharm software platform via the python language. Section 4.1 and Section 4.2 respectively performed experiments and analysis on the super-resolution reconstruction algorithm based on the guided filtering and the improved FMM image restoration algorithm.

4.1. **Experiment and analysis of super-resolution reconstruction algorithm based on guided filtering.** The low-resolution depth map D shown in Figure 2(a) is a depth map with a resolution 320 × 240 obtained by downsampling the actual depth map. Figure 2(b), Figure 2(c), and Figure 2(d) respectively show the experimental results of increasing the resolution of the low-resolution depth map D to 640 × 480 by using bicubic interpolation algorithm, the guided filtering algorithm [17], and the algorithm of this study. Figure 3(a), Figure 3(b) and Figure 3(c) respectively correspond to local enlargements of the red rectangular region in the experimental results of the above algorithm.

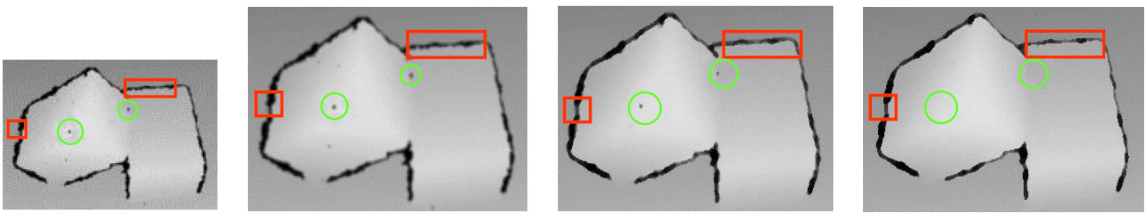

(a) Low-resolution depth map D (b) Bicubic interpolation algorithm (c) Guided filtering algorithm (d) The algorithm of this study

FIGURE 2. Experimental results of resolution reconstruction

(a) Bicubic interpolation algorithm

(b) Guided filtering algorithm

(c) The algorithm of this study

FIGURE 3. Local enlargement of the resolution reconstruction experiment

As shown in Figure 2(a), the original depth map has a low resolution, and the missing depth information in the depth discontinuity region is relatively serious. After processing by the bicubic interpolation algorithm, although the resolution is doubled, the enhanced depth map is not clear due to noise and other factors. The depth map processed by the algorithm in this study and the guided filtering algorithm is both better in terms of clarity than the bicubic interpolation algorithm. However, as shown in Figure 3(b), after processing with the guided filtering algorithm, the pixels are still misestimated in the edge regions where depth information is missing, resulting in blurred edges in the regions where depth information is missing. After processing the algorithm of this study, as shown in Figure 3(c), the edges are relatively clear and there is no blurring of the edges in the regions where depth information is missing.

Table 1 shows the experimental results of enhancing the resolution of the depth map D to $\times 2$, $\times 3$ and $\times 4$ respectively. And, the three algorithms mentioned above are evaluated objectively in terms of Peak Signal-to-Noise Ratio (PSNR), SSIM and Entropy. Generally, the larger the value of the three evaluation criteria, the better the image quality after enhancement. From the value of PSNR, the value of the algorithm in this study is large at different resolutions. From the value of SSIM, there is almost no difference between the values of the three algorithms at different resolutions. And from the value of Entropy, when enhancing the resolution to $\times 2$, the values of the algorithms in this study are larger than the bicubic interpolation algorithm, while there is almost no difference with the guided filtering algorithm. However, when enhancing the resolution to $\times 3$ and $\times 4$, the values of the algorithms in this study are the largest. Therefore, the algorithm of this study is more effective in image enhancement.

Next, a comparison of the green circular region in Figure 2 shows that the dotted depth deficit is still present in Figure 2(b) and Figure 2(c), while the dotted depth deficit is repaired in Figure 2(d). Thus, it is shown that the algorithm for resolution reconstruction

TABLE 1. Comparison of resolution reconstruction algorithms

Methods	Resolution	PSNR[dB]	SSIM	Entropy
Bicubic interpolation	×2	44.136	0.983	7.135
	×3	44.209	0.986	7.128
	×4	44.204	0.986	7.135
Guided filtering	×2	44.952	0.984	7.157
	×3	45.019	0.987	7.142
	×4	44.768	0.987	7.139
The algorithm of this study	×2	45.087	0.982	7.152
	×3	45.213	0.987	7.145
	×4	44.957	0.987	7.142

in this thesis has some repair effect on the absence of depth information in addition to the resolution enhancement effect compared to the bicubic interpolation algorithm and the guided filtering algorithm.

Through the above experiments, it is proved that the super-resolution reconstruction algorithm based on guided filtering can not only improve the resolution of the depth map but also repair the missing depth information in small regions. However, large regions of depth missing in the depth map have not been repaired. And the above algorithm is only able to improve the resolution but not to fill all the depth missing. Therefore, it is necessary to use the algorithm in Section 3.2 to further process the regions with missing depth information to enable better restoration of the depth map. Section 4.2 describes the experimental results and analysis of the algorithm described in Section 3.2.

4.2. **Experiment and analysis of improved FMM image restoration algorithm.** The RGB image D1 with a resolution of 640×480 as shown in Figure 4 and the depth map D3 as shown in Figure 2(d) in Section 4.1 are processed by the restoration algorithm in Section 3.2 to obtain the initially restored depth map D4 as shown in Figure 5. Figure 7 shows the final restored depth map D5 which uses a depth map restoration algorithm based on improved super-resolution and FMM by using weight function in this study. Figure 6 shows the experimental results of the restoration of the depth map D3 of Figure 2(d) using the traditional FMM algorithm. Figure 8 and Figure 9 respectively correspond to the local enlargements of the green rectangular region marked in Figure 5 and Figure 6.

According to Figure 6, it can be seen that the depth map D3 shown in Figure 2(d) has neater edges in the depth discontinuity region after the restoration process by the traditional FMM algorithm, but the sharpness of the edges is lower. Moreover, as shown in Figure 9, the estimation of the missing depth information in the depth discontinuity region produces a large deviation, which leads to a diffusion phenomenon at the edge of the depth discontinuity region. After processing by the improved FMM image restoration algorithm in this study, as shown in Figure 5, the edges of the depth discontinuity region are neater, while the edges are better defined. In addition, as shown in Figure 8, the missing depth information in the depth discontinuity region is estimated more accurately, and the diffusion phenomenon of the edge is diminished. The occurrence of the above situation is strongly related to the value of α in Equation (32). Therefore, this study conducts experiments for the value of α. The data obtained from the experiments are shown in Table 2, and the repaired image obtained is shown in Figure 10. According to the results of the experiment, when $0.55 < \alpha < 1$, the effect of restoration is the best in the edge region where the depth information is missing. Especially when the value α is

FIGURE 4. High-resolution RGB image D1

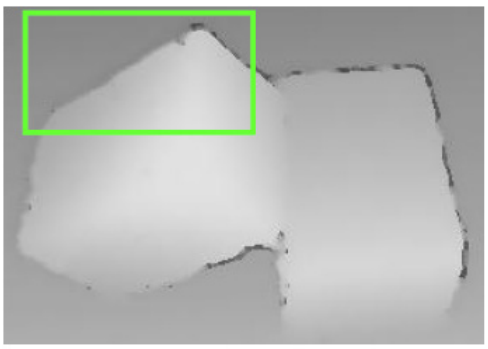

FIGURE 5. Initially restored depth map D4

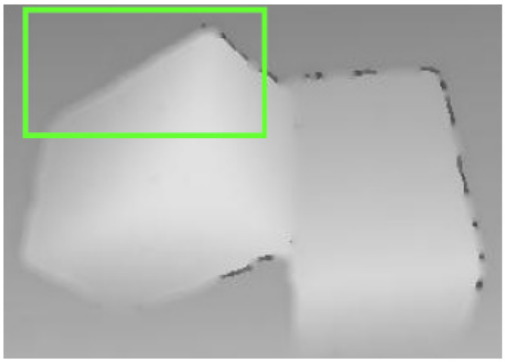

FIGURE 6. Results of the traditional FMM algorithm

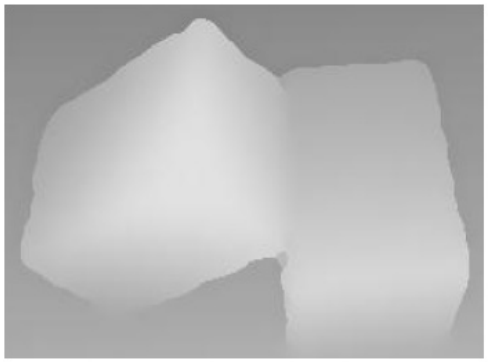

FIGURE 7. Final restored depth map D5

FIGURE 8. Local results of the algorithm in this study

FIGURE 9. Local results of the traditional FMM algorithm

TABLE 2. Results for different values of α

The value of α	$0 < \alpha < 0.55$	$0.55 < \alpha < 1$	$\alpha > 1$
The effect of edges	Diffusion at the edges	Diffusion at the edges is weakening	The estimation is wrong in edges

0.85, the edge will be neither diffused nor blurred. Therefore, α was taken to be 0.85 in this study.

According to the comparison between the final restored depth map D5 shown in Figure 7 and the low-resolution depth map D before image enhancement shown in Figure 2(a), it can be seen that the final repaired depth image D5 not only improves the resolution

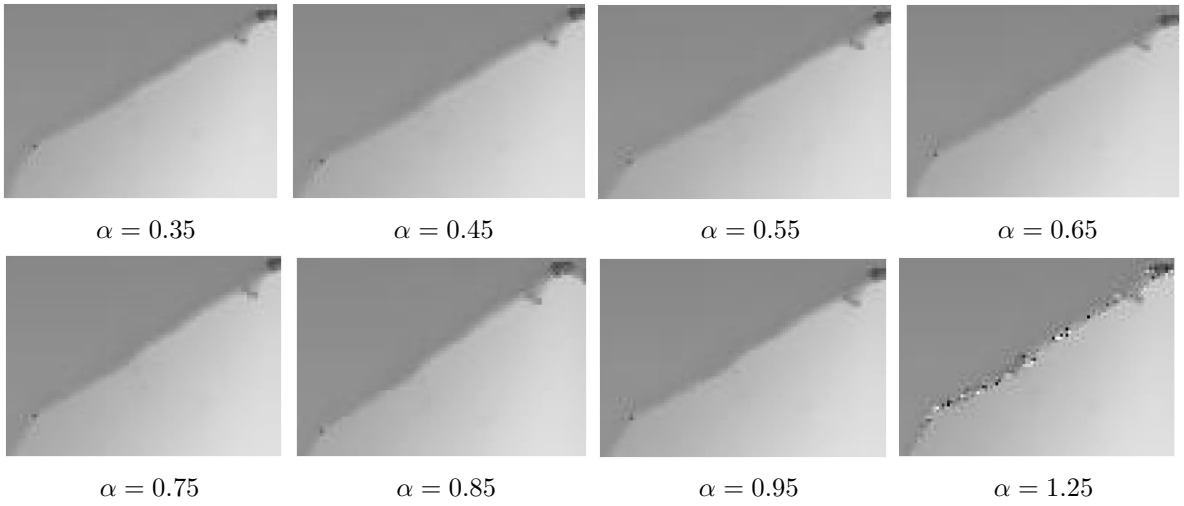

FIGURE 10. Local magnification of α at different values

TABLE 3. Comparison of restoration algorithms

Methods	Resolution	PSNR[dB]	SSIM	RMSE
FMM	×2	44.527	0.971	12.185
	×3	44.088	0.972	13.270
	×4	47.617	0.987	9.087
The algorithm for this study	×2	44.539	0.973	12.068
	×3	44.636	0.978	11.925
	×4	44.676	0.985	8.618

of the depth image, but also maintains the clarity of the image, and better repairs the missing depth information.

In addition, Table 3 shows the experimental results of restoration after enhancing the resolution of the depth map D to ×2, ×3 and ×4, and compares the traditional FMM algorithm and the algorithm of this study in terms of PSNR, SSIM and the Root Mean Square Error (RMSE), respectively. The first two evaluation criteria are as described in Section 4.1, while the evaluation criterion of RMSE is that the smaller the value, the better the image quality after enhancement. According to Table 3, when enhancing the resolution of the depth map D to ×2 and ×3, the algorithm in this study outperforms the traditional FMM algorithm on each of the evaluation criteria. When enhancing the resolution to ×4, it performs poorly on the PSNR, but performs relatively well on both SSIM and RMSE. Therefore, it can be proved that the algorithm of depth map restoration algorithm based on improved super-resolution and FMM by using weight function in this study has a better effect on the restoration.

5. **Conclusion.** Aiming at the problem of low resolution and missing depth information in depth maps obtained by low-resolution depth cameras that are affordable to small and medium-sized manufacturing, this study proposed a depth map restoration algorithm based on improved super-resolution and FMM by using weight function. First, a high-resolution depth map was obtained by super-resolution processing of the low-resolution depth map. Then, the depth information of the enhanced high-resolution depth map was restored by the improvement of the weight function of FMM. In addition, super-resolution processing was used again to repair the missing depth information of the edge caused by the improved FMM. Finally, the effectiveness of this study for depth information

restoration during image enhancement was shown by an experiment which down-samples a depth map of 300,000 pixels taken by a binocular depth camera, then doubles the resolution and repaires the depth information at the same time.

In the future, based on the enhancement and restoration of the depth map in this study, the alignment of the depth map with the edges of the RGB image should be further investigated.

REFERENCES

[1] X. Xiang, Z. Pan and J. Tong, Depth camera in computer vision and computer graphics: An overview, *Journal of Frontiers of Computer Science and Technology*, vol.5, no.6, pp.481-492, 2011.

[2] B. Pan, Q. Fan, X. Cao et al., Depth image inpainting algorithm based on superpixel, *Application Research of Computers*, vol.37, no.6, pp.1863-1867+1870, 2020.

[3] Q. Wan, X. Zhu, G. Chen et al., Research on depth map restoration algorithm based on hierarchical joint bilateral filter, *Computer Engineering and Applications*, vol.57, no.6, pp.184-190, 2021.

[4] H. Zhang, J. Xu and Z. Wang, Probability contour guided depth map inpainting and superresolution using non-local total generalized variation, *Multimedia Tools and Applications*, vol.77, no.7, pp.9003-9020, 2018.

[5] Y. Zhang, L. Ding and G. Sharma, Local-linear-fitting-based matting for joint hole filling and depth upsampling of RGB-D images, *Electron. Imaging*, vol.28, no.3, pp.1-13, 2019.

[6] W. Lin, X. Chen, J. Yang et al., Robust color guided depth map restoration, *IEEE Transactions on Image Processing*, vol.26, no.1, pp.315-327, 2017.

[7] G. Zou, W. Zhang and S. Bian, Fusion of RGB-D images for depth map up-sampling, *Journal of Qingdao University (Natural Science Edition)*, vol.29, no.1, pp.71-74, 2016.

[8] Y. Shin, M. Kim, K.-W. Pak and D. Kim, Practical methods of image data preprocessing for enhancing the performance of deep learning based road crack detection, *ICIC Express Letters, Part B: Applications*, vol.11, no.4, pp.373-379, 2020.

[9] C. Chen, J. Wei, C. Peng et al., Improved saliency detection in RGB-D images using two-phase depth estimation and selective deep fusion, *IEEE Transactions on Image Processing*, vol.29, pp.4296-4307, 2020.

[10] J. Yun, X. Li and W. Xiang, Semantic-guidance multi-scale network for multi-view stereo, *Computer Engineering and Applications*, pp.1-15, 2021.

[11] J. Ku, A. Harakeh and S. L. Waslander, In defense of classical image processing: Fast depth completion on the CPU, *IEEE Conference on Computer and Robot Vision (CRV)*, pp.16-22, 2018.

[12] Y. Liu, H. Zhang, C. Li, H. Zhang and J. Liu, A novel classification & repairing framework for irregular model reconstruction using mass point clouds based on fuzzy inference, *International Journal of Innovative Computing, Information and Control*, vol.15, no.4, pp.1581-1589, 2019.

[13] K. He, J. Sun and X. Tang, Guided image filtering, *IEEE Transactions on Pattern Analysis & Machine Intelligence*, vol.35, no.6, pp.1397-1409, 2013.

[14] A. Telea, An image inpainting technique based on the fast marching method, *Journal of Graphics Tools*, vol.9, no.1, pp.23-34, 2004.

[15] Q. Yang, R. Yang, J. Davis et al., Spatial-depth super resolution for range images, *2007 IEEE Conference on Computer Vision and Pattern Recognition*, pp.1-8, 2007.

[16] Z. Yang, L. Zheng, H. Qu et al., Image denoising research of combining mean filtering with Poisson kernel improved bilateral filtering, *Computer Simulation*, vol.37, no.9, pp.460-463+468, 2020.

[17] B. Chen and X. Tan, Weighted aggregation guided image filtering, *Computer Engineering and Design*, vol.41, no.7, pp.1993-1996, 2020.

Author Biography

Xinyue Xu received the B.Sc. degree from Chizhou College, China. She is currently a M.Eng. student in Information and Electronic Engineering at Zhejiang Gongshang University, China. Her research interests include machine vision and computer vision, such as defect detection for industry, image enhancement and image restoration.

Qingjiu Huang received the B.Sc. degree from Huazhong University of Science and Technology, China; the M.Sc. and Ph.D. degrees from Chiba University, Japan. He is currently a Professor at the Control System Laboratory, Graduate School of Engineering, Kogakuin University, Japan. His research interests include the control theory such as robust control, optimal control, adaptive control, and intelligent control; and the kinematics, dynamics, motion control of multi-joint robot arm, multi-legged robot, biped robot, and four-wheel car.